Model-Based Control of BMEP and NOx Emissions in a Euro VI 3.0L Diesel Engine

2017-24-0057

Model-based Control of BMEP and NOx emissions in a Euro VI 3.0L diesel engine

Roberto Finesso, Omar Marello, Ezio Spessa, and Yixin Yang
Politecnico di Torino

Gilles Hardy
FPT Motorenforschung AG

Abstract

A model-based approach to control BMEP (Brake Mean Effective Pressure) and NOx emissions has been developed and assessed on a FPT F1C 3.0L Euro VI diesel engine for heavy-duty applications. The controller is based on a zero-dimensional real-time combustion model, which is capable of simulating the HRR (heat release rate), in-cylinder pressure, BMEP and NOx engine-out levels. The real-time combustion model has been realized by integrating and improving previously developed simulation tools. A new discretization scheme has been developed for the model equations, in order to reduce the accuracy loss when the computational step is increased. This has allowed the required computational time to be reduced to a great extent. The real-time combustion model has been first calibrated and assessed at both steady-state and transient conditions, on the basis of experimental data acquired at the highly dynamic test bench of ICEAL-PT (Internal Combustion Engines Advanced Laboratory – Politecnico di Torino), in the frame of a research activity in collaboration with FPT Industrial. The model has then been used to realize a model-based control of BMEP and NOx emissions. In particular, the controller provides the injected fuel quantity and the injection timing of the main pulse, for given targets of BMEP and engine-out NOx levels. Finally, the developed controller has been tested on a rapid prototyping device (ETAS ES910) through HiL (Hardware-in-the-Loop) techniques, and demonstrated to have real-time capability.

Introduction

Interest in model-based combustion control has increased in the last few years [1]. A model-based approach for engine control can in fact lead to several advantages compared to the traditional map-based one. For example, the development of a model-based approach requires in general lower experimental effort compared to that required for the calibration of the engine maps, also considering that a large number of engine maps are implemented in modern ECUs (Engine Control Units) [1], which are even difficult to manage. Moreover, a model-based control offers the possibility of optimizing the combustion process onboard, and to adjust the main calibration parameters during the engine operation in real time. For example, this would allow the management of the after-treatment system to be optimized, by setting variable targets of exhaust temperatures and/or pollutant engine-out emissions over a vehicle mission, and these targets may be achieved by adapting the main ECU variables in real-time. In addition, a model-based approach may be capable of taking into account the effects, on the combustion process, of the variability of the environmental conditions (humidity, temperature, pressure) or the effects related to the engine transient operation (turbo-lag, EGR delays, …), without the need of implementing correction maps.

The implementation of model-based controls has been made possible, in the last few years, by the increasing computational performance of modern ECUs.

Therefore, the development of combustion models has become of great interest.

In general, engine simulation can be carried out with different degrees of detail. The main simulation approaches include multidimensional, one-dimensional or zero-dimensional methods, that are characterized by a different degree of detail and computational effort.

3D-CFD (Computer Fluid-Dynamics) methods [2-10] and 1D-CFD approaches [11-16] require a computational time that is not currently suitable to develop model-based combustion controls.

Mean-value engine and combustion models [17-18] are capable of simulating the combustion and emission formation processes with a good level of detail [18]. These methods offer the opportunity of further decreasing the computational time in comparison to 1D-CFD approaches, while guaranteeing at the same time a good predictive capability at steady-state and transient engine operating conditions. Moreover, they are physically consistent, so that they do not require a high calibration effort, and at the same time their accuracy is still acceptable outside the calibration range [18]. Therefore, they can be considered as good candidates for the development of model-based control algorithms. A real-time combustion model, which belongs to this category, has been developed by the authors in [18].

Finally, artificial intelligence systems [19-24], such as support vector machines (SVM), genetic algorithms (GA) and artificial neural networks (ANNs) constitute a last category of models which are often used in the field of engine design and control. These methods do not require the detailed physical knowledge of the investigated process

and are able to capture complex nonlinear system behavior with relatively simple mathematical operations. Moreover, they are characterized by a very small computational time, so that they are good candidates for the development of model-based control algorithms to be implemented in ECUs. However, their training usually requires a high number of experimental tests, and their performance is usually not reliable outside the calibration range.

Contribution of the present study

It should be noted, from the previous background, that mean-value models are among the best candidates for the development of model-based combustion control algorithms, as they are physically consistent, and generally require a low calibration effort and a low computational time.

In this study, a previously developed real-time combustion model [18] has been calibrated and validated for a FPT F1C 3.0L Euro VI diesel engine, and has been used to develop a model-based controller of BMEP and NOx emissions. The activity was carried out in the frame of a research project in collaboration with FPT Industrial.

The real-time combustion model is capable of simulating the HRR (heat release rate) and in-cylinder pressure, along with the related metrics, such as MFB50, PFP (Peak Firing Pressure), IMEP (Indicated Mean Effective Pressure) and BMEP. In particular, the chemical energy release has been simulated using an improved version [18, 25] of the accumulated fuel mass approach, previously presented in [26-30]. A 3-zone thermodynamic model is also included to simulate the in-cylinder burned gas temperatures. The latter model has been enhanced in this paper with respect to previous versions, in order to be able to account for the effect of intake air humidity. Engine-out NOx emissions were simulated on the basis of a semi-empirical correlation, that takes into account the in-cylinder burned gas temperature, as well as MFB50 and additional metrics.

The real-time combustion model used in this study has been improved with respect to previous versions in terms of computational efficiency. In particular, a new discretization scheme has been developed for the in-cylinder pressure model, in order to reduce the accuracy loss when the computational step is increased. This has allowed the required computational time to be reduced to a great extent.

The model has been first calibrated and assessed at both steady-state and transient conditions over several speed/load ramps, on the basis of experimental data acquired at the highly dynamic test bench of ICEAL-PT (Internal Combustion Engines Advanced Laboratory – Politecnico di Torino), in the frame of a research activity in collaboration with FPT Industrial. Then, it has been inverted in order to realize a model-based controller of BMEP and NOx emissions. In particular, the controller is capable of providing the injected fuel quantity and the injection timing of the main pulse, for given targets of BMEP and NOx engine-out emissions.

Finally, the developed controller has been tested on a rapid prototyping device (ETAS ES910) through HiL (Hardware-in-the-Loop), and demonstrated to have real-time capability.

Engine setup and experimental activity

The experimental tests used for model calibration and validation were conducted on a FPT F1C 3.0L Euro VI diesel engine. The main technical specifications of the engine are reported in Table 1.

Table 1. Main technical specifications of the engine.

Engine type	FPT F1C Euro VI diesel engine
Displacement	2998 cm^3
Bore x stroke	95.8 mm x 104 mm
Rod length	160 mm
Compression ratio	17.5
Valves per cylinder	4
Turbocharger	VGT type
Fuel injection system	High pressure Common Rail

The engine (Fig. 1) is equipped with a short-route cooled EGR system, in which the EGR valve is located upstream from the cooler. A flap is installed in the exhaust pipe downstream the turbine, to control the temperature of the exhaust gas flowing to the aftertreatment system and to allow high EGR rates to be obtained when the pressure drop between the exhaust and intake manifolds is not sufficiently high.

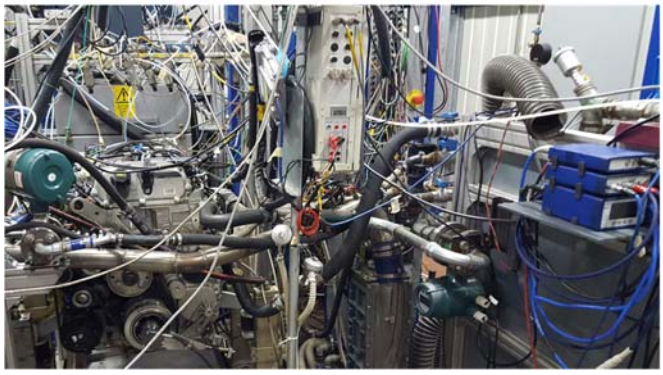

Figure 1. FPT F1C 3.0L Euro VI diesel engine installed on the highly dynamic test bench at the Politecnico di Torino. The rapid prototyping device can be observed on the right side.

The test engine was instrumented with piezoresistive pressure transducers and thermocouples to measure the pressure and temperature at different locations, such as upstream and downstream from the compressor, from the turbine and intercooler, in the intake manifold and in the EGR circuit. Thermocouples were also used to measure the temperatures in each intake and exhaust runners. KISTLER 6058A high-frequency piezoelectric transducers were fitted to the glow-plug seat to measure the in-cylinder pressure time-histories, which were used to realize a pressure-based MFB50 control [1]. The in-cylinder pressure traces were corrected on the basis of the intake pressure that was measured by means of high-frequency KISTLER 4007C piezoresistive transducers, which were located at the inlet runners of the cylinders.

All the experimental tests were carried out on the highly dynamic test bed at ICEAL at the Politecnico di Torino. The test rig is equipped with an ‘ELIN AVL APA 100’ cradle mounted AC dynamometer and

an ‘AVL KMA 4000’, with a reading accuracy of 0.1% over a 0.28-110 kg/h range, to continuously measure the fuel consumption. An ‘AVL AMAi60’ system, consisting of three analyzer trains, was used to measure the engine-out gaseous raw emissions. Two analyzer trains were equipped with complete devices for the analysis of THC, CH4, NOx, and low as well as high CO, CO2 and O2, and were used to measure the intake and exhaust gas composition. All of the abovementioned measurement devices were controlled by a PUMA OPEN 1.3.2 automation system. In order to minimize the testing effort, the test bed environment was interfaced with AVL CAMEO software to run intelligent engine calibration procedures on the basis of the DoE (Design of Experiment) approach.

An ETAS ES910 rapid prototyping device was used to realize pressure-based and model-based controls of the combustion phasing (see [1]), and to test the real-time capability of the model-based controller of BMEP and NOx which has been developed in this study. The main specifications of the ETAS ES910 device are reported in Tab. 2.

Table 2. Main specifications of the ETAS ES910 rapid prototyping device.

Main processor	Freescale PowerQUICC™ III MPC8548 with 800 MHz clock Double precision floating point unit
Memory	512 MByte DDR2-RAM (400 MHz clock) 64 MByte Flash 128 kByte NVRAM

Experimental activity

The experimental tests that have been considered in the present paper include steady-state tests and transient tests. The steady-state tests were mainly used to calibrate the real-time combustion model. To this aim, the following tests were considered (Fig. 2):

- A full engine map with baseline operating parameters, including 123 points.

- EGR-sweep tests at fixed key-points, including 162 points. EGR rate was varied from 0 to 50% by setting different levels of trapped air mass with steps of 50 mg/cycle.

- sweep tests of main injection timing (SOI_{main})/injection pressure (p_f) at fixed key-points, including 125 points. A SOI_{main} variation of ±6 deg around the nominal values and a p_f variation of ±20% around the nominal values were set.

The developed control technique was tested on the engine over different load/speed ramps. Details on these ramps are reported in the “Results and discussion” section.

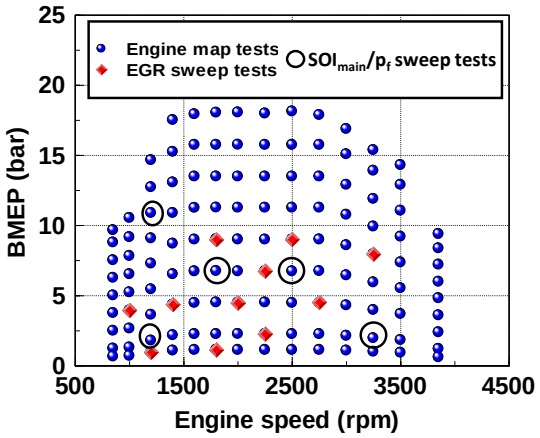

Figure 2. Experimental tests used for the calibration of the real-time combustion model.

Real-time combustion model

The real-time combustion model that has been used for the development of the BMEP/NOx controller includes the simulation of:

1. Chemical energy release: the approach is based on an enhanced version [25] of the model previously presented by the authors, which was based on the accumulated fuel mass approach [30]. The input data of the model are the injection parameters, as well as the main thermodynamic conditions in the intake manifold and the engine operating parameters.

2. In-cylinder pressure: the approach is based on the inversion of a single-zone heat release model [31] which requires the net energy release as input; the latter is derived starting from the predicted chemical energy release and estimating the heat transfer between the charge and the walls. Polytropic evolutions are assumed during the compression and expansion phases. Several metrics, such as PFP and IMEP, can be extracted from the simulated in-cylinder pressure.

3. Friction losses: the Chen-Flynn approach has been used to predict FMEP on the basis of the engine speed and peak firing pressure; the simulation of friction losses allows BMEP to be evaluated starting from IMEP.

4. Pumping losses: the pumping losses (PMEP) were simulated on the basis of a semi-empirical correlation which takes into account the intake and exhaust manifold pressure levels, as well as engine speed.

5. NOx emission levels: an improved version of the semi-empirical correlation previously developed by the authors for a 2.0L Euro 5 diesel engine and reported in [32] has been tuned and validated for the 3.0L F1C Euro VI engine considered in the present study.

The detailed description of the combustion model and the calibration methodology is reported in [18]. However, a summary is provided hereafter for the sake of clarity. Moreover, the correlations of the model parameters which have been obtained from the model recalibration on the F1C engine have also been reported.

Figure 3 reports the scheme of the real-time combustion model.

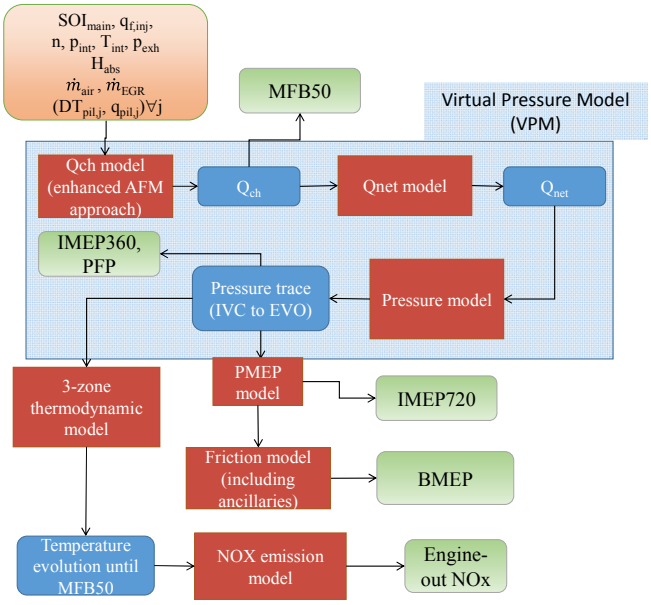

Figure 3. Scheme of the real-time combustion model.

Estimation of the chemical energy release Q_{ch} and of the net energy release Q_{net}

The equations of the Q_{ch} and Q_{net} sub-models are reported in Table 3. The reader may refer to [18] for further details related to these equations.

Table 3. Main equations of the Q_{ch} and Q_{net} models.

Qch model	$\frac{dQ_{ch,pil,j}}{dt}(t) = K_{pil,j}\left[Q_{fuel,pil,j}(t-\tau_{pil,j}) - Q_{ch,pil,j}(t)\right]$ $\frac{dQ_{ch,main}}{dt}(t) = K_{1,main}\left[Q_{fuel,main}(t-\tau_{main}) - Q_{ch,main}(t)\right] + K_{2,main}\frac{dQ_{fuel,main}(t-\tau_{main})}{dt}$ $Q_{fuel,j}(t) = \int_{t_{SOI,j}}^{t} \dot{m}_{f,inj}(t) H_L dt \qquad t \le t_{EOI,j}$ $Q_{fuel,j}(t) = \int_{t_{SOI,j}}^{t_{EOI,j}} \dot{m}_{f,inj}(t) H_L dt \qquad t > t_{EOI,j}$ $Q_{ch} = \sum_{j=1}^{n} Q_{ch,j}$ where j indicates the generic injection pulse, H_L indicates the fuel lower heating value, K and τ are the combustion rate coefficient and ignition delay coefficient of the Q_{ch} model.
Qnet model	$Q_{net,ht} \cong Q_{ch}\frac{m_{f,inj}H_L - Q_{ht,glob}}{m_{f,inj}H_L}$ $Q_{net} \cong Q_{net,ht} - Q_{f,evap}$ where $Q_{f,evap}$ and $Q_{ht,glob}$ indicate the fuel evaporation heat from SOI to SOC (J) and the heat exchanged by the charge with the walls over the combustion cycle (J), and $m_{f,inj}$ is the total injected fuel mass per cyc/cyl

The Q_{ch} and Q_{net} models were assessed for the steady-state conditions reported in Fig. 2. Physically-consistent correlations were identified for the model calibration parameters, as a function of the in-chamber thermodynamic quantities at SOI/SOC (start of injection/start of combustion) and other engine variables, as follows:

$$K_{pil}[\frac{1}{\deg}] = 2.73E-04\, p_f^{-0.7887}\, O_2^{1.90} n^{0.452} q_{pil,tot}^{-0.239} \quad (1)$$

$$K_{1,main}[\frac{1}{\deg}] = 7.78E-8 \cdot SOI_{main}^{2.16}\, p_{int}^{0.55} O_2^{0.937} n^{-0.159} q_{f,inj}^{-0.274} \quad (2)$$

$$K_{2,main}[-] = 0.567 p_f^{0.215} \rho_{SOC,main}^{-1.13} O_2^{0.0926} n^{-0.0484} q_{main}^{0.401} \quad (3)$$

$$\tau_{pil}[\deg] = 1.31 p_f^{0.0496} \rho_{SOIP}^{-1.16}\, n^{0.606} O_2^{-0.0298} \quad (4)$$

$$\tau_{main}[\deg] = 7.71 p_f^{-0.789} \rho_{SOI,main}^{-2.46} n^{1.41} q_{f,inj}^{0.259} \quad (5)$$

$$Q_{f,evap}[kJ] = 3.75E-6\; T_{int}^{1.17} n^{0.227} q_{f,inj}^{-0.162} \quad (6)$$

$$Q_{ht,glob}[kJ] = 1.701E3 \cdot SOI_{main}^{-2.06}\, p_{int}^{-0.466} O_2^{0.465} n^{-0.351} q_{f,inj}^{1.29} \quad (7)$$

In equations (1-7), ρ_{SOI}, ρ_{SOC} indicate the in-chamber densities evaluated at the start of injection or combustion, respectively, and are expressed in kg/m^3. The injection pressure p_f is expressed in bar, the engine speed n in rpm, the total injected fuel quantity $q_{f,inj}$ (used as a load parameter) in mm^3/cyc/cyl, the total injected fuel quantity of the pilot shots $q_{pil,tot}$ in mm^3/cyc/cyl and finally the intake oxygen concentration O_2 in %. T_{int} and p_{int} indicate the intake manifold temperature and pressure, respectively.

Estimation of the in-cylinder pressure

The equations of the in-cylinder pressure sub-model are reported in Table 4. The reader may refer to [18] for further details related to these equations.

Table 4. Main equations of the in-cylinder pressure model.

Pressure model	Starting condition (pIVC): $p_{IVC} = p_{int} + \Delta p_{int}$ Compression phase (IVC to SOC): $pV^m = const$ Combustion phase (SOC to EOC): $p^i = \frac{\Delta Q_{net} - \frac{p^{i-1}}{2}(V^i - V^{i-1}) + \frac{1}{\gamma - 1}p^{i-1}V^{i-1}}{\frac{V^i - V^{i-1}}{2} + \frac{V^i}{\gamma - 1}}$ Expansion phase (EOC to EVO): $pV^{m'} = const$ where p_{int} indicates the intake manifold pressure, pIVC the in-cylinder pressure at IVC, m and m' the compression and expansion polytropic exponents.

With reference to table 4, the in-chamber pressure was evaluated, during the combustion interval, on the basis of the inversion of a

single-zone heat release model, which can be summarized as follows [31]:

$$dQ_{ch} - dQ_{ht} = dQ_{net} = pdV + mC_v dT \qquad (8)$$

where Q_{ht} represents heat transfer and C_v the specific heat at constant volume. In Eq. (8) the last term is usually rewritten using the ideal-gas law and assuming a constant mass m, so that:

$$dQ_{net} = pdV + \frac{1}{\gamma - 1} d(pV) \qquad (9)$$

where $\gamma = c_p/c_v$. The last differential in Eq. (9) is typically rewritten in terms of pressure and volume differentials, and the following differential equation is commonly proposed in the literature [31]:

$$dQ_{net} = \frac{\gamma}{\gamma - 1} pdV + \frac{1}{\gamma - 1} Vdp \qquad (10)$$

In the previous versions of the combustion model proposed by the authors [25, 30], the pressure differential was evaluated on the basis of Eq. (10), as follows:

$$dp = \left(\frac{\gamma - 1}{V}\right)\left(dQ_{net} - \frac{\gamma}{\gamma - 1} pdV\right) \qquad (11)$$

which had been then discretized according to the following scheme:

$$p^i = p^{i-1} + \frac{\left[Q_{net}^i - Q_{net}^{i-1} - \frac{\gamma}{\gamma - 1} p^{i-1}(V^i - V^{i-1})\right](\gamma - 1)}{V^i} \qquad (12)$$

The new approach proposed in this study starts directly from Eq. (9) and is based on the following discretization scheme:

$$Q_{net}^i - Q_{net}^{i-1} = \Delta Q_{net} = \frac{p^i + p^{i-1}}{2}(V^i - V^{i-1}) + \frac{1}{\gamma - 1}(p^i V^i - p^{i-1} V^{i-1}) \qquad (13)$$

so that the pressure value at time instant t^i is evaluated as follows:

$$p^i = \frac{\Delta Q_{net} - \frac{p^{i-1}}{2}(V^i - V^{i-1}) + \frac{1}{\gamma - 1} p^{i-1} V^{i-1}}{\frac{V^i - V^{i-1}}{2} + \frac{V^i}{\gamma - 1}} \qquad (14)$$

The new approach for pressure discretization has allowed the accuracy loss to be reduced to a great extent when the computational step is increased.

A comparison of the model accuracy (quantified by the RMSE, i.e., root mean squared error) when using the new scheme (i.e., Eq. (14)) and the old one (i.e., Eq. (12)) is reported in Table 5, for different values of the computational step. It can be seen that the new discretization scheme leads to a virtually negligible loss of accuracy in terms of IMEP and BMEP prediction, when the crank angle integration step (CAstep) is increased to 0.5 or 1 deg, starting form a nominal value of 0.1 deg.

Table 5. Comparison between the values of RMSE for the main quantities of the real-time combustion model, when using the old (a) and new (b) pressure discretization schemes. Engine map tests are considered.

CAstep	0.1	0.2	0.5	1
RMSE MFB50 (deg)	0.85	0.85	0.87	0.90
RMSE PFP (bar)	2.94	2.96	3.04	3.71
RMSE IMEP360 (bar)	0.21	0.23	0.42	0.83
RMSE IMEP720 (bar)	0.20	0.23	0.42	0.83
RMSE BMEP (bar)	0.17	0.22	0.44	0.85
RMSE NOx (ppm)	37.0	36.9	37.1	37.9

(a) Old discretization scheme for pressure

CAstep	0.1	0.2	0.5	1
RMSE MFB50 (deg)	0.85	0.85	0.87	0.90
RMSE PFP (bar)	2.92	2.93	**2.93**	**2.94**
RMSE IMEP360 (bar)	0.21	0.21	**0.21**	**0.22**
RMSE IMEP720 (bar)	0.21	0.21	**0.21**	**0.21**
RMSE BMEP (bar)	0.17	0.17	**0.17**	**0.17**
RMSE NOx (ppm)	36.9	36.7	36.7	36.3

(b) New discretization scheme for pressure

In Eq. (14) the isentropic coefficient $\gamma = c_p/c_v$ was set constant and equal to 1.37.

The following correlations were identified for the pressure model parameters, which are functions of the intake manifold thermodynamic conditions and of the engine load and speed:

$$m = 2.136 T_{int}^{-0.0696} n^{0.0074} q_{f,inj}^{0.0022} \qquad (15)$$

$$m' = 1.321 \cdot T_{int}^{0.0532} n^{-0.0272} q_{f,inj}^{-0.0312} \qquad (16)$$

$$\Delta p_{int}[bar] = 0.0929\, p_{int}^{1.15} n^{0.032} q_{f,inj}^{-0.0319} \qquad (17)$$

The in-cylinder pressure trace has been simulated over the compression and combustion phases only, and this allows the gross IMEP (i.e., IMEP360) to be estimated. Pumping losses were evaluated by means of a dedicated correlation, which is reported in the next section.

The simulation of the in-cylinder pressure traces also allows peak-firing pressure (PFP) to be evaluated.

Estimation of PMEP and FMEP

The following correlation was identified to evaluate PMEP for the engine considered in this study:

$$PMEP[bar] = 0.01248 \cdot p_{exh}^{1.068} n^{0.557} - 0.0337 \cdot p_{int}^{1.18} n^{0.402} \qquad (18)$$

The Chen-Flynn approach [33] was adopted to estimate FMEP.

The experimental values of FMEP were evaluated as the difference between the experimental values of the net IMEP and the measured values of BMEP, as follows:

$$FMEP = IMEP - BMEP \quad (19)$$

The values of IMEP of one of the four cylinders were taken as being representative of all the cylinders, due to the low cylinder-to-cylinder dispersion.

The following correlation was identified to evaluate FMEP for the engine considered in this study:

$$FMEP[bar] = -0.2679 + 6.177E-4 \cdot n - 5.164E-8 \cdot n^2 + 0.00584 \cdot PFP \quad (20)$$

where the engine speed is expressed in rpm and PFP is expressed in bars.

The squared correlation coefficient R^2 between the predicted and experimental values of FMEP is the order of 0.9.

Estimation of the NOx emissions

The engine-out NOx emissions were evaluated starting from the semi-empirical model developed by the authors in [32]. That correlation has been re-tuned for the engine considered in the present study, on the basis of the experimental tests reported in Fig. 2.

The following correlations were obtained from the tuning of the NOx emission model:

$$NO_x\,[ppm] = 1135 \exp^{\frac{6.78e+03}{MFB50}} \exp^{\frac{-4.69e+04}{T_{b,MFB50}}} O_2^{-1.99}\, n^{-0.430}\, q_{f,inj}^{0.568} \quad (21)$$
$$(q_{f,inj} \le 45mm^3, n \le 1900rpm)$$

$$NO_x\,[ppm] = 5698 \exp^{\frac{3.40e+03}{MFB50}} \exp^{\frac{-4.37e+04}{T_{b,MFB50}}} O_2^{1.55}\, n^{-0.138}\, q_{f,inj}^{0.306} \quad (22)$$
$$(q_{f,inj} > 45mm^3, n \le 1900rpm)$$

$$NO_x\,[ppm] = 4042 \exp^{\frac{5.20e+03}{MFB50}} \exp^{\frac{-4.82e+04}{T_{b,MFB50}}} O_2^{0.724}\, n^{-0.334}\, q_{f,inj}^{0.583} \quad (23)$$
$$(q_{f,inj} \le 45mm^3, n > 1900rpm)$$

$$NO_x\,[ppm] = 64.74 \exp^{\frac{2.92e+03}{MFB50}} \exp^{\frac{-3.44e+04}{T_{b,MFB50}}} O_2^{2.80}\, n^{-0.353}\, q_{f,inj}^{0.372} \quad (24)$$
$$(q_{f,inj} > 45mm^3, n > 1900rpm)$$

Equations (21-24) were derived considering all the data related to the engine map, EGR-sweep and SOI_{main}/p_f sweep tests, as it was verified that this led to satisfactory results for all datasets. Moreover, at the beginning, all the main engine variables related to NOx formation were included in the correlations, and a sensitivity analysis was carried out in order to exclude the least influential ones.

In order to avoid discontinuities when applying the NOx model, Eqs. (21-24) have been calibrated using overlapping calibration datasets. In other words, each of the four calibration datasets also included tests characterized by injected quantities and speed levels exceeding the breakpoints (i.e., $q_{f,inj}$ = 45 mm^3, n = 1900 rpm).

It can be seen that the temperature of the burned gases evaluated at MFB50 (i.e., $T_{b,MFB50}$) has been used. The temperature of the burned gases was evaluated by means of the real-time thermodynamic three-zone model that is described in the next section. The evaluation of the $T_{b,MFB50}$ term, in general, requires the evaluation of the in-cylinder pressure, which is an input of the thermodynamic model.

Moreover, it can be seen that the MFB50 parameter has also been used in the correlation. It was verified that the use of MFB50 leads to a significant increase in the NOx prediction accuracy for all the experimental datasets.

Three-zone thermodynamic model

A refined version of the real-time three-zone thermodynamic model presented in [34] has been used in order to evaluate the temperature of the burned gases. In particular, the model has been refined by taking into account the effect of the intake air humidity. The 3-zone thermodynamic model is based on the splitting of the in-chamber content into a vapor-fuel zone (f), an unburned gas zone (u), made up of fresh-air, residual gas and EGR, and a burned gas zone (b) obtained from a globally stoichiometric combustion process. Energy and mass conservation equations are applied to each zone (see Table 6).

Table 6. Energy and mass conservation equations of the 3-zone thermodynamic model.

3-zone thermodynamic model	$\delta Q_{ht,f} + V_f dp = d\left(m_f h_f\right) - dm_{f,inj} h_{f,inj} + dm_{f\to b} h_f$ $\delta Q_{ht,u} + V_u dp = d\left(m_u h_u\right) + dm_{u\to b} h_u$ $\delta Q_{ht,b} + V_b dp = d\left(m_b h_b\right) - dm_{u\to b} h_u - dm_{f\to b} h_f$ $dm_f = dm_{f,inj} - dm_{f\to b}$ $dm_u = -dm_{u\to b}$ $dm_b = dm_{u\to b} + dm_{f\to b}$ Arrows indicate a mass transfer between adjacent zones. $dm_{f,inj}$ is the injected fuel mass in the time interval dt, $\delta Q_{ht,j}$ is the infinitesimal heat transfer between the j^{th} zone and the in-chamber walls. The 'h' symbol indicates the specific enthalpy.

The burned gas zone is considered to be made up of CO_2, H_2O, O_2, N_2, O, H, OH and NO, and the dissociation effects are therefore taken into account for accurate calculation of the burned gas temperatures. It has been verified in [34] that second-order polynomial correlations are able to accurately describe the specific enthalpy of the different zones, as follows:

$$h_j = a_j T_j^2 + b_j T_j + c_j \quad (25)$$

The values of the coefficients of the enthalpy terms were improved with respect to those reported in [34]. In particular, in previous papers the correlations for the enthalpy of the burned and unburned gases were derived assuming a value of the intake air humidity H_{abs} = 10 g_v/kg_a, and the effect of humidity on NOx emissions was taken

into account by adopting the standard correction formulas. In this paper, the effect of humidity has been directly taken into account in the definition of the enthalpies, as shown in Table 7, in order to improve the physical consistency of the approach.

The heat transfer terms in the equations reported in Tab. 6 were estimated by means of a convective and a radiative contribution, as explained in [34], the first one being modeled by the Woschni correlation.

On the basis of the procedure reported in [34], the energy and mass conservation equations are then discretized considering finite time intervals $\Delta t = t^i - t^{i-1}$. It is thus possible to explicitly derive the temperature of the three zones by solving the resulting second-order polynomial equations for the three zones.

The unknowns can therefore be solved in closed form without an iterative procedure, and this allows a very low computational effort to be obtained.

Table 7. Summary of the coefficients used in Eq. (25) to estimate the enthalpies of the burned zone (b), unburned zone (u) and fuel zone (f). In the table, H_{abs} indicate the absolute humidity, $X_{r,tot}$ the total residual + EGR ratio in the combustion chamber, λ the relative air-to-fuel ratio

a_u	$0.09983 + \frac{0.0121}{50}(Habs - 10)$
b_u	$982.3 + \frac{32.32}{50}(Habs - 10)$
c_u	$-477140 \quad -2817105\frac{X_{r,tot}}{\lambda} + \frac{-657505 + \frac{X_{r,tot}}{\lambda \cdot 0.6} \cdot 107783.7}{50}(Habs - 10)$ $X_{r,tot} = \frac{mEGR + mres}{mEGR + mres + mair + mfuel}$
a_b	$0.595\frac{200 - p(bar)}{150} + 0.425\frac{p(bar) - 50}{150} + \frac{\left[0.0597\frac{200 - p(bar)}{150} + 0.0344\frac{p(bar) - 50}{150}\right]}{50}(Habs - 10)$
b_b	$-882.854\frac{200 - p(bar)}{150} \quad -233.624\frac{p(bar) - 50}{150} + \frac{\left[-180.43\frac{200 - p(bar)}{150} \quad -75.549\frac{p(bar) - 50}{150}\right]}{50}(Habs - 10)$
c_b	$-1436077.57\frac{200 - p(bar)}{150} \quad -2050200.15\frac{p(bar) - 50}{150} + \frac{\left[-274618\frac{200 - p(bar)}{150} \quad -380570\frac{p(bar) - 50}{150}\right]}{50}(Habs - 10)$
a_f	1.4459
b_f	860.78
c_f	-949736

Model-based control of BMEP and NOx

A model-based approach to control BMEP and NOx emissions has been developed in this study. The controller is based on the inversion of the real-time combustion model reported in the previous section, in order to predict the values of the injected fuel quantity $q_{f,inj}$ and of the injection timing of the main pulse, i.e., SOI_{main}, that allows desired targets of BMEP and engine-out NOx emissions to be reached. SOI_{main} has been selected as the control variable for the NOx emissions control due to its capability to realize a cycle-by-cycle engine response, while the EGR rate (whose dynamics is slower) has been kept constant and equal to the setpoint value. The model was inverted by adopting an iterative procedure, in which the first run was based on the initial assumption of the $q_{f,inj}$ and SOI_{main} control variables and a cycle-based integral control was applied to adjust the control variable value in order to attain convergence of the target variables (i.e., $BMEP_{tgt}$ and NOx_{tgt}). The iterative procedure stops when the difference between the predicted values and required values of the target variables fall below the predefined thresholds ε_{BMEP} and ε_{NOx}.

More in detail, the model inversion has been carried out according to the following procedure. Target values of BMEP and NOx, i.e., $BMEP_{tgt}^j$ and NOx_{tgt}^j, are set for a given cycle 'j'. The first model run is carried out using the nominal engine map values for the $q_{f,inj}$ and SOI_{main} control variables.

The predicted values of BMEP and NOx for the generic iteration 'i', i.e., $BMEP_i^j$ and NOx_i^j, are compared with the target values $BMEP_{tgt}^j$ and NOx_{tgt}^j. The errors between the target and the actual values for the iteration 'i' are then estimated as follows:

$$Err_{BMEP,i}^j = BMEP_{tgt}^j - BMEP_i^j \qquad (26)$$

$$Err_{NOx,i}^j = NOx_{tgt}^j - NOx_i^j \qquad (27)$$

SOI_{main} is then corrected on the basis of NOx error, while $q_{f,inj}$ is corrected on the basis of BMEP error and a new iteration is carried out. This choice is justified by the fact that the sensitivity of BMEP to $q_{f,inj}$ is much greater than the sensitivity to SOI_{main}, and the sensitivity of NOx to SOI_{main} is greater than the sensitivity to $q_{f,inj}$ (at least when the BMEP error is small and $q_{f,inj}$ is not far from the value which allows the BMEP target to be obtained). It should be noted that the combustion model is obviously able to estimate the combined effects of SOI_{main} and $q_{f,inj}$ variations on both BMEP and NOx emissions during a given iteration, therefore the choice of controlling BMEP using $q_{f,inj}$ only and of controlling NOx using SOI_{main} only just affects the number of iterations needed to achieve convergence and does not affect the accuracy in the estimation of BMEP and NOx levels.

With reference to the SOI_{main} correction scheme, a preliminary estimation of the sensitivity of NOx emissions with respect to SOI_{main} is needed. To this end, Eqs. (21-24) are used to estimate how NOx emissions change when setting an MFB50 variation with respect to a reference value, keeping constant all the other parameters (i.e., $T_{b,MFB50}$, O_2, n, $q_{f,inj}$). A NOx sensitivity factor with respect to MFB50 variation, i.e., S_{NOx}^j, is calculated as follows:

$$S_{NOx}^{j} = \frac{\Delta NOx^{j}}{\Delta MFB50^{j}} \qquad (28)$$

The value of SOI_{main} for the subsequent iteration (i+1) is then obtained adopting the following correction scheme:

$$SOI_{main,i+1}^{j} = SOI_{main,i}^{j} + K_{NOx,i}^{j} \frac{Err_{NOx,i}^{j}}{S_{NOx}^{j}} \qquad (29)$$

where $K_{NOx,i}^{j}$ is a modulation factor that was introduced in order to optimize the response of the controller and to guarantee stable operations. An optimal strategy for the definition of the $K_{NOx,i}^{j}$ parameter was identified. In particular, the value of $K_{NOx,i}^{j}$ was limited to the [0.15-2] range, and was varied, iteration by iteration, as a function of the sign of the error between two consecutive iterations, according to the following method:

$$K_{NOx,i}^{j} \in [0.15, 2]$$
$$if \ \ sign\left(Err_{NOx,i}^{j}\right) = sign\left(Err_{NOx,i,i-1}^{j}\right): \quad K_{NOx,i}^{j} = K_{NOx,i-1}^{j} \cdot 2 \qquad (30)$$
$$if \ \ sign\left(Err_{NOx,i}^{j}\right) \neq sign\left(Err_{NOx,i-1}^{j}\right): \quad K_{NOx,i}^{j} = \frac{K_{NOx,i-1}^{j}}{2}$$

With reference to the correction of $q_{f,inj}$, a similar correction scheme has been used:

$$q_{f,inj,i+1}^{j} = q_{f,inj,i}^{j} + K_{BMEP,i}^{j} \cdot \frac{Err_{BMEP,i}^{j}}{S_{BMEP,i}^{j}} \qquad (31)$$

where $S_{BMEP,i}^{j}$ is a BMEP-to-fuel sensitivity factor which is derived from the average engine fuel conversion efficiency, and $K_{BMEP,i}^{j}$ is a modulation factor, with is defined as follows:

$$K_{BMEP,i}^{j} \in [0.1, 1]$$
$$if \ \ sign\left(Err_{BMEP,i}^{j}\right) = sign\left(Err_{BMEP,i-1}^{j}\right): \quad K_{BMEP,i}^{j} = K_{BMEP,i-1}^{j} \cdot 2 \qquad (32)$$
$$if \ \ sign\left(Err_{BMEP,i}^{j}\right) \neq sign\left(Err_{BMEP,i-1}^{j}\right): \quad K_{BMEP,i}^{j} = \frac{K_{BMEP,i-1}^{j}}{2}$$

The strategy for the modulation of the factors $K_{NOx,i}^{j}$ and $K_{BMEP,i}^{j}$ was inspired by a previous closed-loop MFB50 controller, which was presented by the authors in [1]

Figure 4 shows the model inversion scheme.

It should be noted that, in this study, the variables n, p_{int}, T_{int}, DT, q_{pil} and the air mass flow rate were obtained from the engine sensors (i.e.., these variables were available from the ECU), while H_{abs} and p_{exh} were obtained from test bench sensors. With reference to the EGR mass flow rate, the experimental value derived from intake manifold CO_2 concentration was used for model calibration and validation in steady-state conditions. Instead, a look-up table was used for the transient simulations, which was built using the nominal EGR rate values obtained from the steady-state engine map tests.

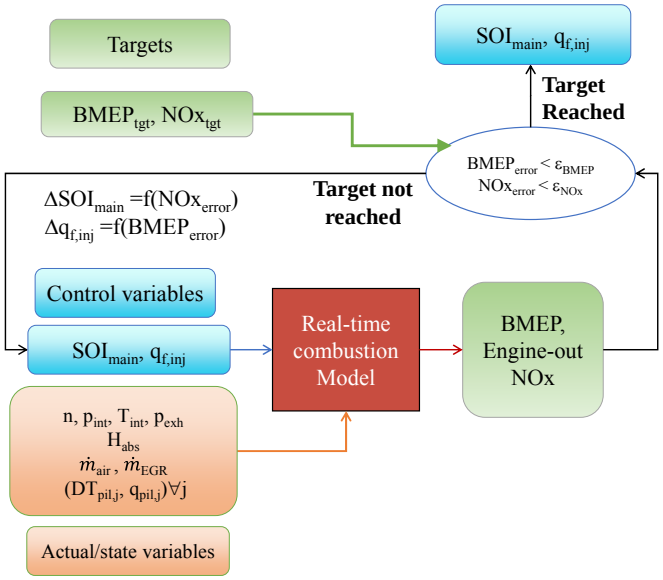

Figure 4. Flow chart of the BMEP/NOx controller.

Results and discussion

Assessment of the real-time combustion model: steady state tests

First, the accuracy of the real-time combustion model has been assessed for the steady state tests reported in Fig. 2. All the results shown in this section were obtained adopting a crank angle computational step of 0.1 deg. However, it was shown in Table 5 that the loss of accuracy is virtually negligible when increasing this step to 1 deg. The adoption of the latter step is associated to a computational time that is compatible for real-time applications.

Figure 5 reports the predicted vs. experimental values of MFB50, while Fig. 6 reports the predicted vs. experimental values of PFP, IMEP720 (i.e., net IMEP) and BMEP, and finally Fig. 7 reports the predicted vs. experimental values of engine-out NOx emissions, for all the tests reported in Fig. 2. The prediction accuracy of each model has been quantified by the squared correlation coefficient (R^2) and by the Root Mean Squared Error (RMSE), which are reported in each figure.

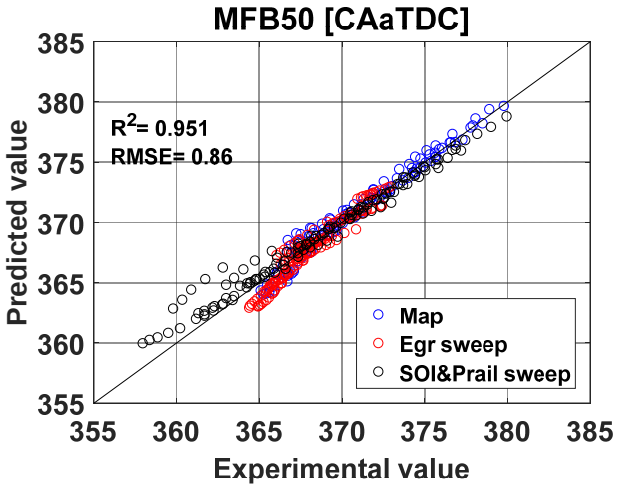

Figure 5. Predicted vs. experimental MFB50 values for the steady-state tests reported in Fig. 2.

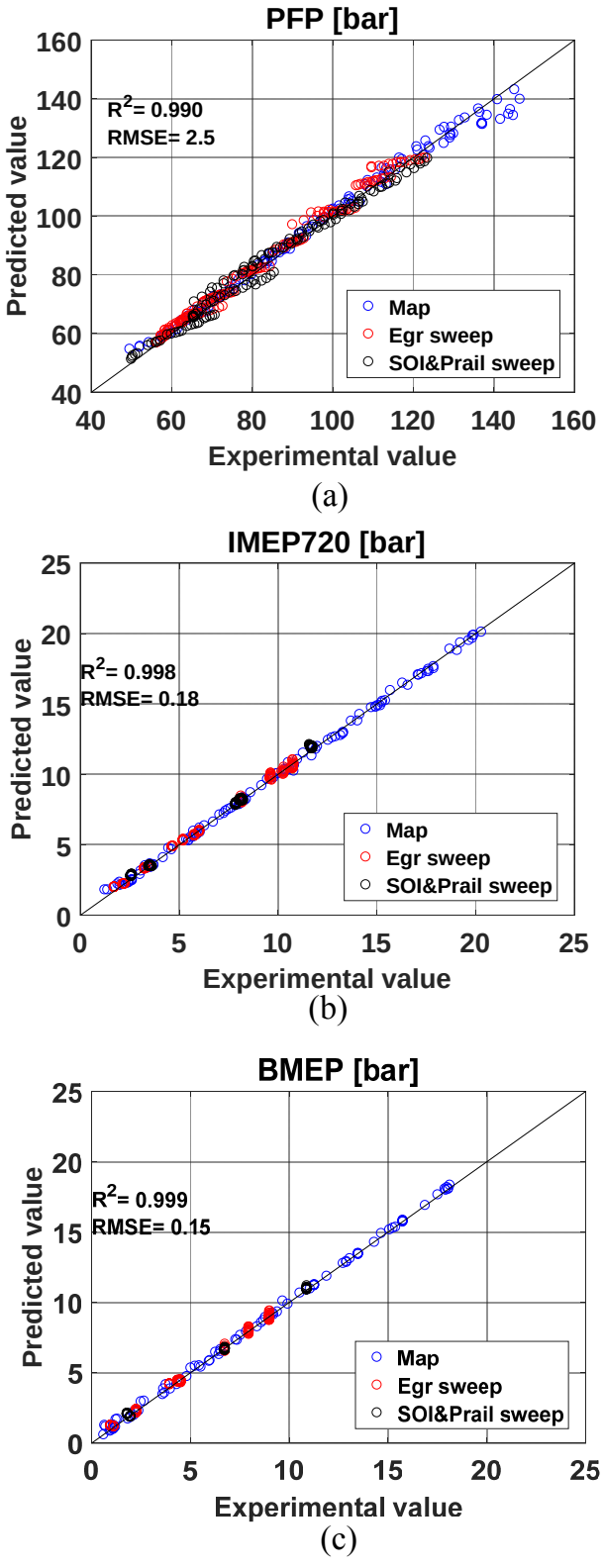

Figure 6. Predicted vs. experimental values of PFP (a), IMEP720 (b) and BMEP (c) for the steady-state tests reported in Fig. 2.

With reference to MFB50 prediction, it can be seen in Fig. 5 that the RMSE of the physical model is of the order of 0.9 deg and that the

dispersion of the predicted values remains in an acceptable range for all the test categories. With reference to Fig. 6, it can be noted that a very accurate prediction of PFP is obtained (RMSE=2.5 bar), as well as of IMEP720 (RMSE=0.18 bar) and of BMEP (RMSE = 0.15 bar). The model is robust not only for the engine map tests with nominal values of engine calibration parameters, but also when EGR, injection timing and injection pressure are varied at fixed operating condition. This confirms its physical consistency.

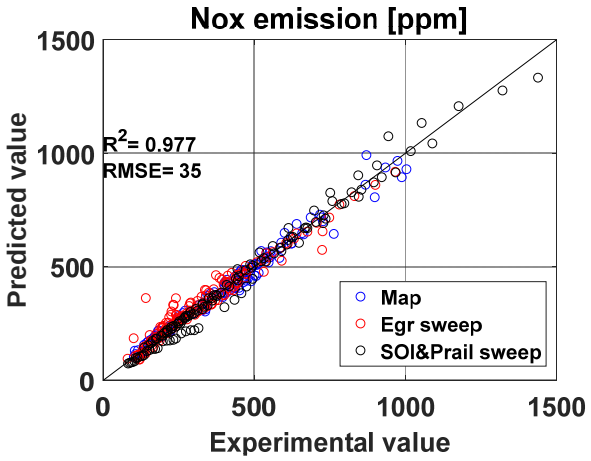

Figure 7. Predicted vs. experimental values of engine-out NOx emissions for the steady-state tests reported in Fig. 2.

With reference to the prediction of NOx emissions (Fig. 7), the RMSE is of the order of 35 ppm, and the model accuracy is good for all the considered test categories.

Validation of the real-time combustion model: transient tests

The real-time combustion model has then been validated in transient conditions. The results reported in this section are related to six sets of up/down speed/load ramps of different duration. Figure 8 reports the time histories of the engine speed and torque for the six analyzed sets of ramps. The engine speed variation range was between 1600 rpm and 2500 rpm, while the engine torque variation range was between 55 Nm and 215 Nm. The duration of the first three sets of ramps is 5s, while the duration of the remaining three sets of ramps is 3s. It can be seen in Fig. 8 that the first test is constituted by a ramp-up and a ramp-down of both engine speed and torque, the second test is constituted by a ramp-up and a ramp-down of torque at fixed engine speed, while the third test is constituted by a ramp-up and a ramp-down of speed at fixed engine torque. The three sets of ramps have then been repeated by reducing the ramp duration to 3s.

The main model results have been reported in Figs. 9-12. In particular, the figures report the predicted and experimental values of MFB50 and PFP (Fig. 9a, 9b), of BMEP (Fig. 10), of the instantaneous engine-out NOx emissions (Fig. 11) and of the cumulated engine-out NOx emissions (Fig. 12). In all the charts, the experimental values have been reported in blue color, while the results of the model have been reported in red color. The values of RMSE are also reported at the top of each graph.

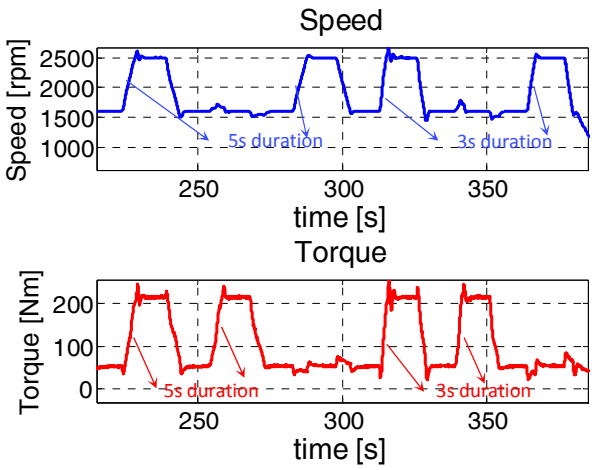

Figure 8. Engine speed and torque as a function of time for the analyzed transient test.

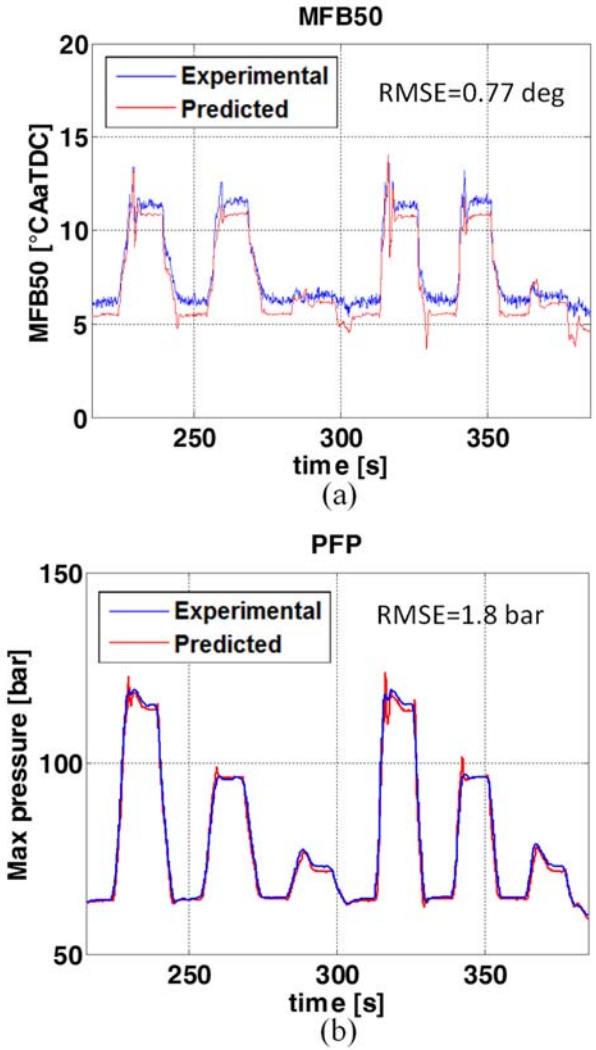

Figure 9. Predicted and experimental trends of MFB50 (a) and PFP (b) for the analyzed transient test.

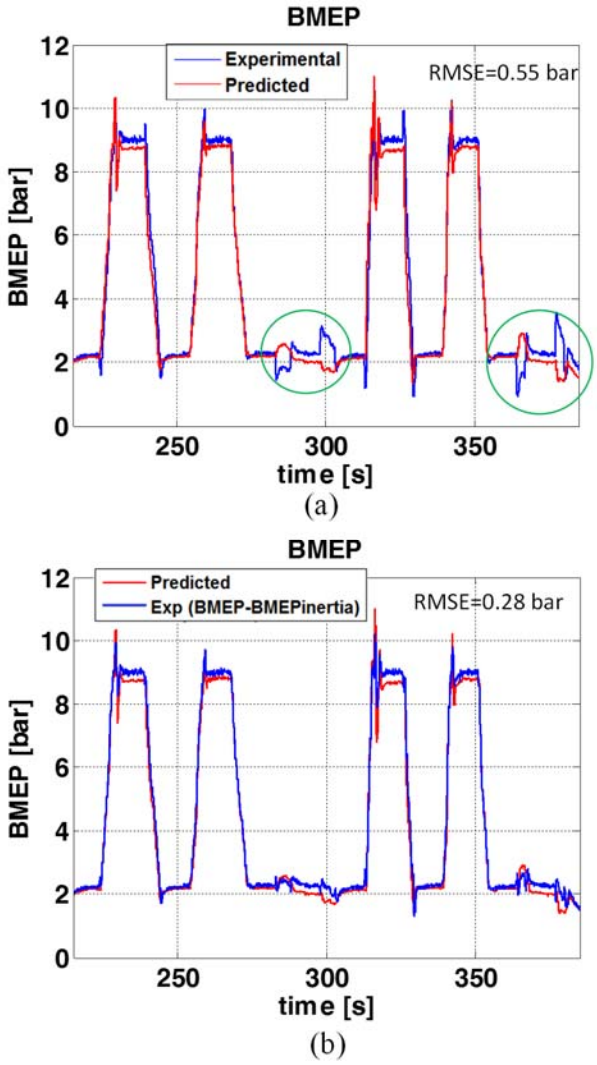

Figure 10. Predicted and experimental trends of BMEP for the analyzed transient test. a: raw experimental BMEP trace is reported. b: the engine inertial term was subtracted from the raw experimental BMEP trace.

With reference to the prediction of the MFB50 and peak-firing pressure, it can be seen in Fig. 9 that the model accuracy is satisfactory, as the RMSE values are of the order of 0.8 deg and 1.8 bar, respectively. This suggests that the prediction of the heat release and of the in-cylinder pressure trace is accurate over the considered transient tests.

With reference to the prediction of BMEP (Fig. 10), a preliminary comparison between the predicted and raw experimental trends revealed some discrepancies (see Fig. 10a), especially over the speed ramps at constant torque (highlighted with a red circle in Fig. 10a), and the values of RMSE was of the order of 0.55 bar. It was found that these BMEP peaks represent the inertial contribution due to the engine speed variation. Therefore these terms are not related to fuel injection. If the inertial term (i.e., J dω/dt, where J is the engine moment of inertia and ω is the engine angular speed) is subtracted from the raw experimental BMEP trace, a better agreement is observed (see Fig. 10b) between the experimental and predicted trends of BMEP, as the RMSE value decreases to a value of 0.28 bar.

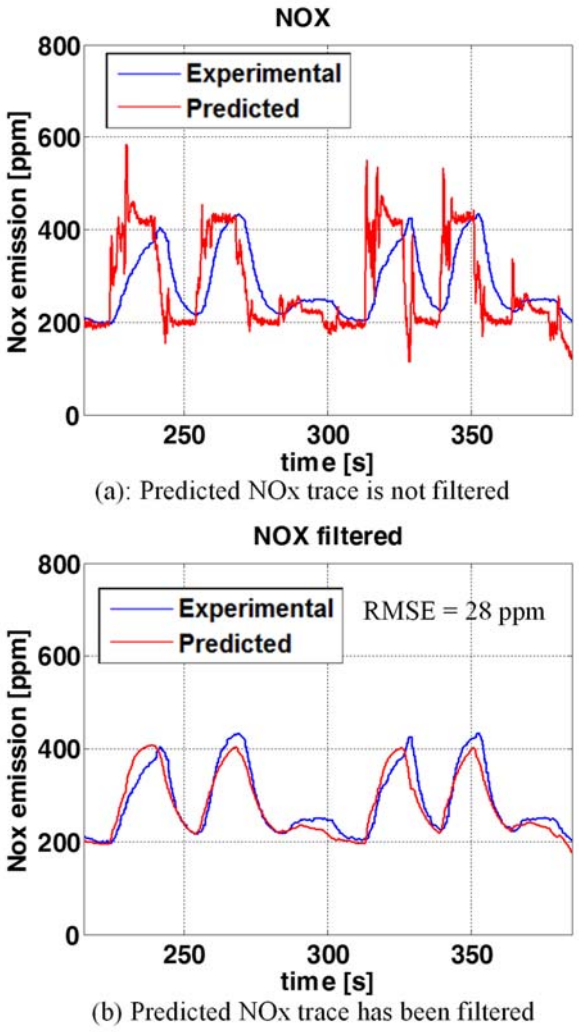

Figure 11. Predicted and experimental trends of engine-out NOx emissions for the analyzed transient test. a: the original predicted NOx trace is reported. b: the predicted NOx trace has been filtered using a time constant of 5s.

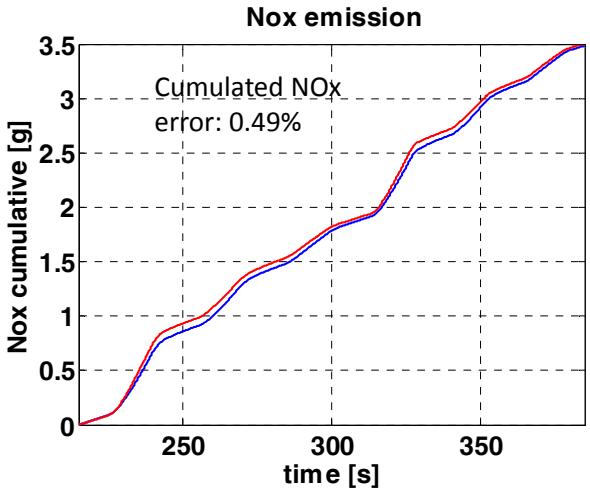

Figure 12. Predicted and experimental trend of cumulated engine-out NOx emissions for the analyzed transient test.

With reference to the prediction of the instantaneous engine-out NOx emissions (Fig. 11), a preliminary comparison between the predicted and the experimental trends also revealed some discrepancies (see Fig. 11a). In particular, the experimental trend seems to be much smoother than the predicted one, as though it was a result of a time filtering. In order to check this effect, the predicted NOx trend has been filtered over time using the Matlab function 'filter'. It was found that a time constant τ_c=5s leads to the best agreement between the predicted and experimental engine-out NOx trends, as can be seen in Fig. 11b (RMSE = 28 ppm). The physical reason of the time filtering of the experimental NOx trace may be due to the mixing of the exhaust gases that occurs in the pipes between the engine and the exhaust gas analyzer of the test bench. Therefore, the NOx emission trend obtained from the measurement of the exhaust gas analyzer seems not to be representative of the actual dynamics which occurs in the exhaust manifold of the engine. In order to check this effect, a NOx sensor with high frequency response (not available for the considered tests) should be installed in the engine.

Figure 12 reports the comparison between the experimental and predicted trends of the cumulated engine-out NOx emissions, where the predicted trace was obtained using the filtered predicted NOx instantaneous emissions (i.e., those reported in Fig. 11b). A good agreement is observed, as the cumulated error is of the order of 0.5%.

Sensitivity analysis to input variables

A sensitivity analysis has been carried out, for the engine map steady-state tests, in order to check the effect of deviations in the actual/state input variables with respect to the nominal values. The results are reported in Table 8. In particular, Table 8 reports, for each model outcome, the deviation in the values of the RMSE with respect to the baseline case, in which the nominal values of the input variables are used.

Table 8. Sensitivity analysis of the main model outcomes with respect to deviations in the input state variables. The table reports, for each model outcome, the deviation in the values of the RMSE with respect to the baseline case, in which the nominal values of the input variables are used. x: virtually no effect.

	Δ	MFB50 [deg]	PFP [bar]	IMEP360 [bar]	IMEP720 [bar]	BMEP [bar]	NOx [ppm]
p_{int}	+7%	< 0.1	< 5	x	<0.1	<0.1	< 50
p_{int}	-7%	<0.1	< 5	<0.1	<0.1	<0.1	< 50
T_{int}	+2%	x	x	x	x	x	x
T_{int}	-2%	x	x	x	x	x	x
p_{exh}	+7%	No effect	No effect	No effect	<0.1	<0.1	x
p_{exh}	-7%	No effect	No effect	No effect	<0.1	<0.1	x
p_f	+4%	x	x	x	x	x	< 10
p_f	-4%	x	x	x	x	x	x
Air mass	+5%	x	x	x	x	x	< 10
Air mass	-5%	x	x	x	x	x	< 10
EGR mass	+5%	x	x	x	x	x	< 10
EGR mass	-5%	x	x	x	x	x	< 10

BMEP/NOx controller

Steady-state conditions

The controller of BMEP and NOx is based on the inversion of the real-time combustion model, according to the scheme reported in Fig. 4. In particular, the controller is able to predict the values of the injected fuel quantity $q_{f,inj}$ and of the main injection timing SOI_{main} that allow desired targets of BMEP and engine-out NOx emissions to be reached.

This approach has been validated at steady-state conditions over the engine map tests and SOI_{main}/p_f sweep tests shown in Fig. 2. EGR-sweep tests has not been considered, as the NOx variation in those tests was obtained through EGR variation and not SOI_{main} variation. In particular, the experimental values of BMEP and NOx emissions were set as targets of the controller, and the values of $q_{f,inj}$ and SOI_{main} predicted by the controller were compared to the real actuated values. Constant values of $q_{f,inj}$ and SOI_{main} were set as initial conditions. The results are shown in Figs. 13 and 14. In particular, Fig. 13 reports the predicted vs. experimental values of injected fuel mass, while Fig. 14 reports the predicted vs. experimental values of SOI_{main}.

The inverted model is highly accurate in estimating the injected quantity, as the RMSE values are of the order of 0.7 mg/stroke and 0.5 mg/stroke for the engine map tests and SOI_{main}/p_f sweep tests, respectively (Fig. 13).

With reference to the estimation of SOI_{main}, the inverted model accuracy is good, as the RMSE values are of the order 1.4 deg and 0.75 deg for the engine map tests and SOI_{main}/p_f sweep tests, respectively (Fig. 14). However, with reference to the engine map tests (Fig. 14a), a larger dispersion is shown in some regions of the map. It was verified that the larger dispersion occurs especially at lower loads. This larger dispersion may be explained as follows. First, at lower loads the absolute values of NOx emissions are generally low (some tens of ppm), and therefore the relative error of the NOx model becomes significant. Second, at lower loads the sensitivity of NOx variation with respect to SOI_{main} variation is much lower than for higher loads. Both effects have an impact on the accuracy in the values of SOI_{main} predicted by the inverted model.

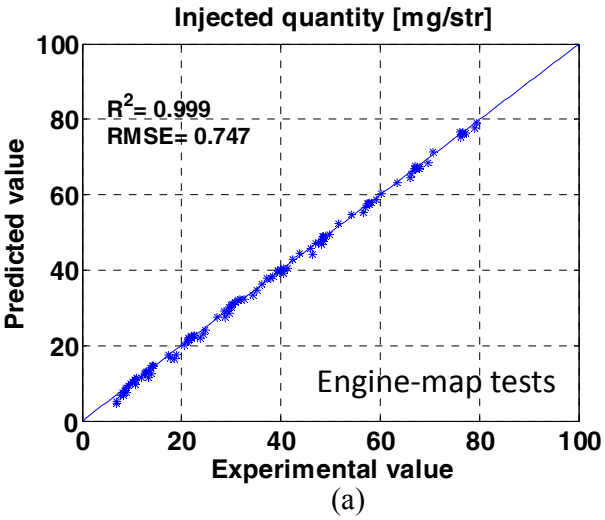

(a)

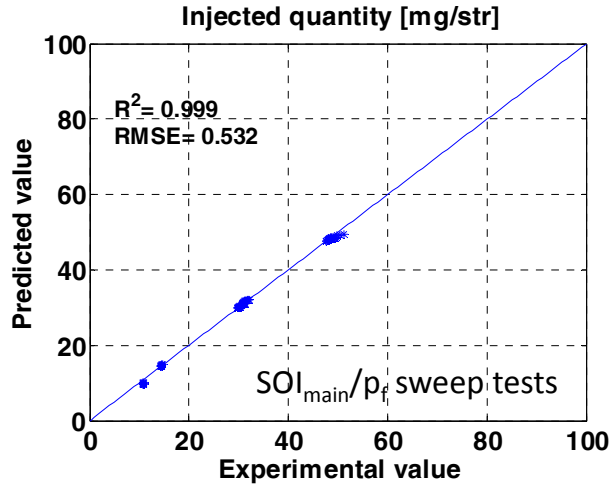

(b)

Figure 13. Inverted model: predicted vs. experimental values of injected fuel mass for the engine map tests (a) and SOI_{main}/p_f sweep tests (b) shown in Fig. 2. The experimental values of BMEP were set as targets.

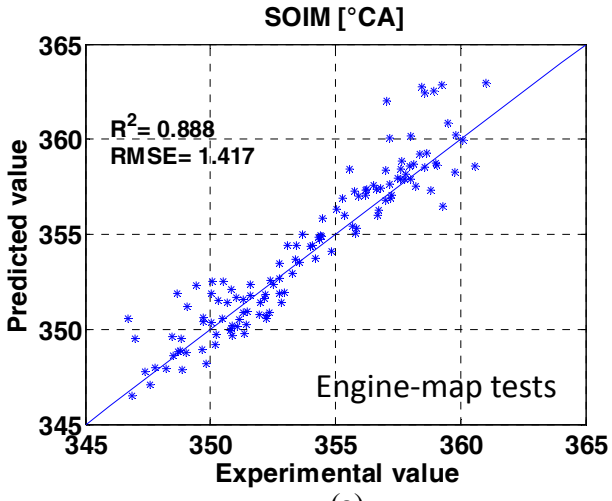

(a)

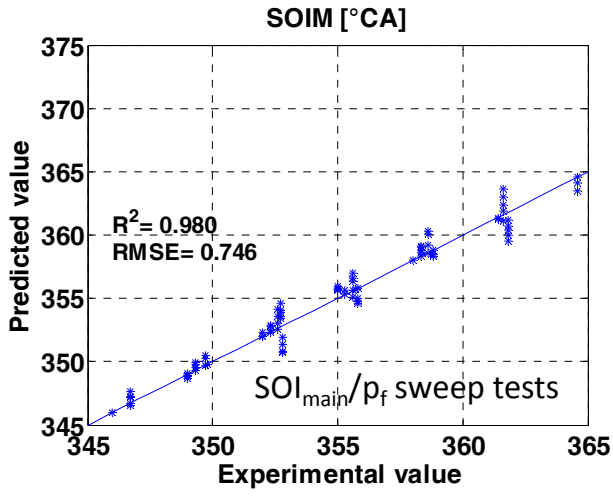

(b)

Figure 14. Inverted model: predicted vs. experimental values of SOI_{main} for the engine map tests (a) and SOI_{main}/p_f sweep tests (b) shown in Fig. 2. The experimental values of NOx emissions were set as targets.

The sensitivity of NOx variation with respect to SOI_{main} variation has been calculated for the experimental SOI_{main}/p_f sweep tests shown in Fig. 2, and the results are reported in Fig. 15 for a high-load key-point (Fig. 15a) and a low-load key-point (Fig. 15b). In particular, the figure reports the values of $\Delta NOx/\Delta SOI_{main}$ as a function of ΔSOI_{main}, that is, the difference between the actual value of SOI_{main} during the sweep test and the nominal value of SOI_{main} for the given key-point. The results indicate a much larger sensitivity of NOx with respect to ΔSOI_{main} for the higher-load point (up to 60-80 ppm/deg), and a smaller sensitivity for the low-load key-point (10-20 ppm/deg). Moreover, it can be seen in Fig. 15 that the sensitivity of NOx is not symmetrical with respect to a positive or negative variation of SOI_{main}: an advance in injection timing has a larger impact on NOx variation than a delay.

The previous analysis suggests that a SOI-based control of NOx emissions is more effective for medium-high load conditions than for low-load conditions.

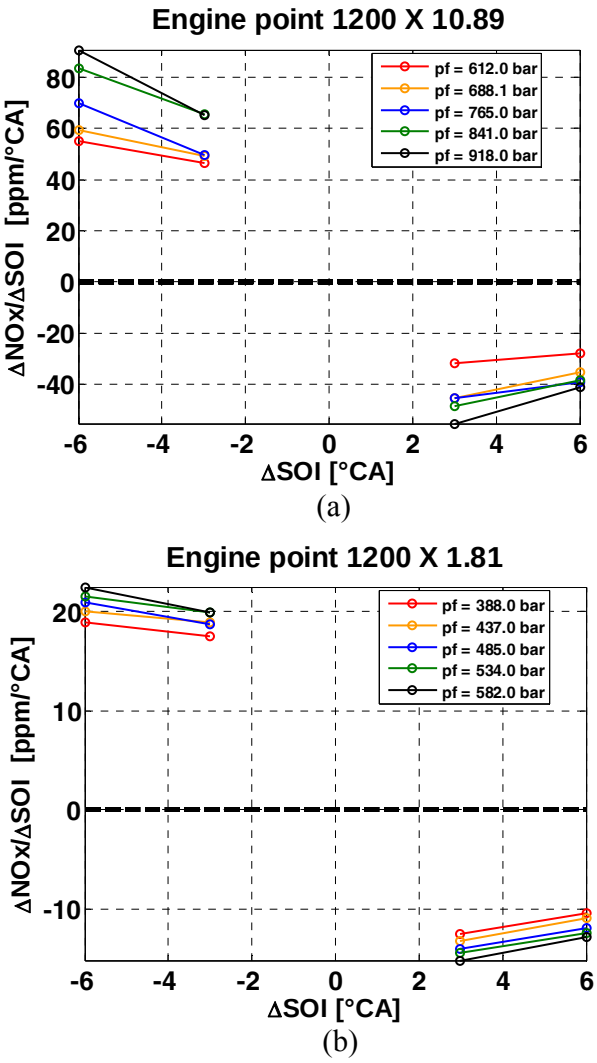

Figure 15. $\Delta NOx/\Delta SOI_{main}$ as a function of ΔSOI_{main} for the experimental SOI_{main}/p_f sweep tests shown in Fig. 2. Negative values of ΔSOI_{main} indicate that SOI is anticipated with respect to the nominal SOI_{main}value for the considered key-point.

Transient conditions

With reference to transient conditions, only the BMEP controller could be tested over the ramps shown in Fig. 8. In particular, the experimental values of BMEP were set as targets, and the predicted fuel quantities were compared to the experimental ones. The SOI_{main} values were instead kept equal to the nominal values derived from the engine maps. In fact, the NOx controller could not be tested, as the measured NOx emissions trends were found not to be representative of the actual engine-out levels (see Fig. 11), due to a smoothing effect that may be related to the mixing of the exhaust gases in the pipes between the engine and the gas analyzer of the test bench. Therefore, the measured NOx emission trends could not be set as targets for the NOx controller. The results of the BMEP controller are shown in Fig. 16, which reports the predicted vs. experimental values of the injected fuel mass (Fig. 16a), as well as the comparison between the experimental BMEP values, which were set as targets, and the predicted BMEP values obtained from model inversion. Fig. 16a shows that the BMEP controller accuracy is good, as the RMSE value of the injected fuel quantity is equal to 1.1 mg/stroke, while Fig. 16b confirms that the BMEP targets have been achieved over the transient.

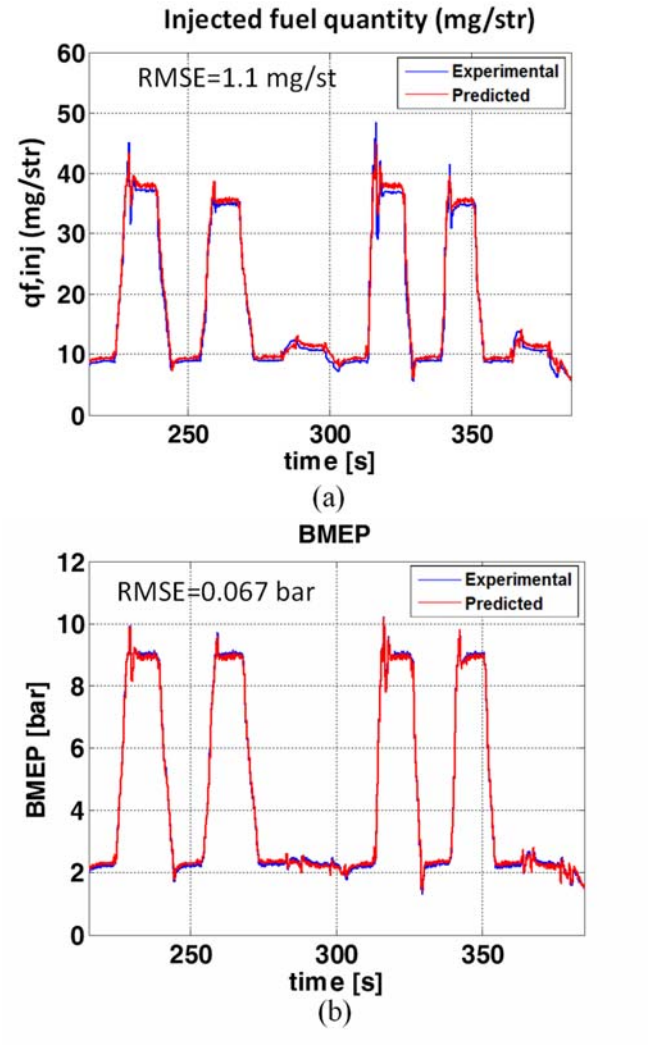

Figure 16. a: predicted and experimental values of the injected fuel mass when testing the BMEP controller over the ramps shown in Fig. 8. b: predicted and experimental values of BMEP over the same ramps.

Number of iterations required for model inversion

The number of iterations required for model inversion depends on the initial conditions for $q_{f,inj}$ and SOI_{main} and on the error thresholds ε_{NOX}, ε_{BMEP} (see Fig. 4). With reference to the results reported in Figs. 13-16, error thresholds of 0.1 bar for BMEP and 20 ppm for NOx emissions were set to stop the iterative process. It was verified that, on average, 3-4 iterations are required if the initial conditions of $q_{f,inj}$ and SOI_{main} are derived from the nominal engine-map values, while about 6 iterations are required if the initial conditions of $q_{f,inj}$ and SOI_{main} are set as constant values. Therefore, it may be advantageous to set the nominal engine map-based values as initial conditions in order to minimize the number of required iterations.

HiL and computational time

The BMEP/NOx control was developed in Matlab/Simulink environment and was then implemented on a rapid prototyping (RP) device (i.e., ETAS ES910), through ETAS Intecrio software, in order to perform Hardware-in-the-Loop testing and to check the computational time required by the control. The RP device was coupled to a real-time engine emulator represented by an NI PXI device equipped with a real-time engine model (see [1]).

The aim of this phase was to test the real-time capability of the controller, for the subsequent implementation on the real engine. The rapid prototyping activity on the engine is currently ongoing and the results will be shown in a future paper.

The results of the HiL activity, in terms of computational time required by the controller on the ETAS ES910 device per iteration, are shown in Table 9.

Table 9. a: average computational time required for the calculation of the main outcomes of the combustion model, when implemented on the ETAS ES910 RP device. The reported times are progressive (e.g., the time required to evaluate NOx also includes the time required to evaluate MFB50 and pressure-related metrics). b: average computational time required for the calculation of the NOx emissions, using different integration steps in the 3-zone thermodynamic model. The analysis was made considering engine map tests.

Calculated quantity	RMSE (CAstep= 1.0 deg)	Average computational time, per iteration, on ETAS ES910 device. The reported computational time values are cumulative.
MFB50	0.90 deg	≈200 µs
PFP	2.94 bar	≈350 µs
IMEP360	0.22 bar	≈350 µs
IMEP720	0.21 bar	≈350 µs
BMEP	0.17 bar	≈350 µs
NOx	36 ppm	≈1400 µs

(a)

CA step used in the the 3-zone thermodynamic model (CAstep for HRR and pressure is kept at 1.0 deg)	RMSE NOx	Average computational time, per iteration, on ETAS ES910 device.
1.0	36 ppm	≈1400 µs
2.0	36 ppm	≈950 µs
3.0	36 ppm	≈780 µs
4.0	36 ppm	≈710 µs
5.0	40 ppm	≈650 µs

(b)

In particular, Tab. 9a reports the average computational time required for the calculation of the main outcomes of the real-time combustion model per iteration, when implemented on the ETAS ES910 RP device, along with the RMSE values. A crank angle integration step of 1.0 deg was used. The reported times are progressive (e.g., the time required to evaluate NOx also includes the time required to evaluate MFB50 and pressure-related metrics).

It should be noted that this analysis has been carried out considering the engine map tests only, therefore the RMSE values are slightly different from those reported in Figs. 5-7, which refer to the whole experimental dataset.

It can be seen that the required computational time to evaluate the heat release and pressure-related metrics is quite low, i.e., about 350 µs per iteration. The total required computational time to estimate NOx is instead of the order of 1.4 ms per iteration, due to the 3-zone thermodynamic model that is time consuming.

A sensitivity analysis was made in order to verify the impact of using a larger computational step for the 3-zone thermodynamic model, by keeping the computational step of the heat release and pressure models equal to 1.0 deg. The results are shown in Table 9b, and indicate that it may be possible to adopt a step of 4 deg without any accuracy loss in the estimation of NOx emissions (at least at steady-state conditions), and this leads to a reduction in the total required computational time to a value of about 700 µs per iteration.

Future work

The BMEP/NOx controller is going to be tested on the engine installed at the test bench through rapid prototyping, and the results will be shown in the near future. Moreover, the controller will be further developed by including additional control variables, such as EGR and boost pressure.

Summary/Conclusions

A model-based approach to control BMEP (Brake Mean Effective Pressure) and NOx emissions has been developed and assessed on a FPT F1C 3.0L Euro VI diesel engine for heavy-duty applications. The controller provides the injected fuel quantity and the timing of the main pulse, for given targets of BMEP and engine-out NOx levels. The controller is based on the inversion of a zero-dimensional real-time combustion model, which is capable of simulating the HRR (heat release rate) and in-cylinder pressure (along with the related metrics, such as MFB50, IMEP, BMEP) as well as the NOx engine-out levels. A 3-zone thermodynamic model has been used to estimate the burned gas temperatures, which are required by the NOx model.

The work has been carried out in the frame of a research activity in collaboration with FPT Industrial, and the experimental data were acquired at the highly dynamic test bench of ICEAL-PT (Internal Combustion Engines Advanced Laboratory – Politecnico di Torino).

First, the real-time combustion model has been calibrated and assessed at both steady-state and transient conditions, over some speed/load ramps. It was verified that the model provides an accurate estimation of the combustion metrics and NOx emissions, as the values of RMSE (root mean squared error) are of the order of 0.9 deg for MFB50, 0.18 bar for IMEP, 0.15 bar for BMEP and 35 ppm for NOx emissions, at steady-state conditions. The accuracy does not change significantly in transient operation.

The model has then been inverted in order to realize the BMEP/NOx controller. The latter has been tested at steady-state conditions, using the experimental values of BMEP and NOx emissions as targets. The predicted values of injected quantity and injection timing of the main pulse have been compared with the experimental ones, and a good accuracy was found. In particular, the RMSE value of the injected quantity was of the order of 0.5-0.7 mg/stroke, while the RMSE value of the main injection timing was of the order of 0.7-1.4 deg.

Finally, the controller has been implemented on a rapid prototyping device (ETAS ES910) and tested in Hardware-in-the-Loop in order to check its real-time capability. It was found that a computational time of 700 μs per iteration can be achieved using a computational step of 1 deg for the pressure model and of 4 deg for the 3-zone thermodynamic model, without any significant deterioration in the model accuracy with respect to the baseline case, in which an integration step of 0.1 deg is adopted. This result was also achieved by adopting a new numerical discretization scheme for the in-cylinder pressure model, which allowed the computational step to be relaxed with a virtually negligible loss of accuracy in the calculation of the pressure-related metrics and NOx emissions.

The developed controller will be tested on the engine installed at the test bench in the near future, through rapid prototyping.

References

1. Finesso, R., Maier, C., Marello, O., Misul, D.A., et al., "Development and Assessment of Pressure-Based and Model-Based Techniques for the MFB50 Control in a Euro VI 3.0L HD Diesel Engine", SAE Int. J. Engines 10(4):2017, doi:10.4271/2017-01-0794.
2. D'Errico, G., Frassoldati, A., Hardy, G., Lucchini, T., et al., "Modeling Non-Premixed Combustion Using Tabulated Kinetics and Different Fame Structure Assumptions", SAE Technical paper 2017-01-0556, doi: 10.4271/2017-01-0556
3. D'Errico, G., Lucchini, T., Maghbouli, A., Najafabadi, M.I., et al., "Numerical Investigation of PPCI Combustion at Low and High Charge Stratification Levels", SAE Technical paper 2017-01-0739, doi: 10.4271/2017-01-0739
4. Fontanesi, F., Giacopini, M., "Multiphase CFD-CHT optimization of the cooling jacket and FEM analysis of the engine head of a V6 diesel engine", *Applied Thermal Engineering* 52 : 293-303, 2013, doi: 10.1016/j.applthermaleng.2012.12.005.
5. Jemni, M.A., Kantchev, G., Abid, M.S., "Influence of intake manifold design on in-cylinder flow and engine performances in a bus diesel engine converted to LPG gas fuelled, using CFD analyses and experimental investigations.", *Energy* 36:2701-2715, 2011, doi: 10.1016/j.energy.2011.02.011.
6. Lee, C.H., Reitz, R.D., "CFD simulations of diesel spray tip penetration with multiple injections and with engine compression ratios up to 100:1", *Fuel* 111:289–297, 2013, doi: 10.1016/j.fuel.2013.04.058.
7. Perini, F., Dempsey, A., Reitz, R., Sahoo, D. et al., "A Computational Investigation of the Effects of Swirl Ratio and Injection Pressure on Mixture Preparation and Wall Heat Transfer in a Light-Duty Diesel Engine", SAE Technical Paper 2013-01-1105, 2013, doi:10.4271/2013-01-1105.
8. Rakopoulos, C.D., Kosmadakis, G.M., Pariotis, E.G., "Investigation of piston bowl geometry and speed effects in a motored HSDI diesel engine using a CFD against a quasi-dimensional model", *Energy Conversion and Management* 51:470–484, 2010, doi: 10.1016/j.enconman.2009.10.010.
9. Mobasheri, R., Peng, Z., Mirsalim, S.M., "Analysis the effect of advanced injection strategies on engine performance and pollutant emissions in a heavy duty DI-diesel engine by CFD modeling", *International Journal of Heat and Fluid Flow* 33:59–69, 2012, doi: 10.1016/j.ijheatfluidflow.2011.10.004.
10. Cipolla, G., Vassallo, A., Catania, A., Spessa, E. et al., "Combined application of CFD modeling and pressure-based combustion diagnostics for the development of a low compression ratio high-performance diesel engine" SAE Technical Paper 2007-24-0034, 2007, doi:10.4271/2007-24-0034.
11. Lešnik, L., Iljaz, J., Hribernik, A., Kegl, B., "Numerical and experimental study of combustion, performance and emission characteristics of a heavy-duty DI diesel engine running on diesel, biodiesel and their blends", *Energy Conversion and Management* 81:534–546, 2014, doi: 10.1016/j.enconman.2014.02.039.
12. Kéromnès, A., Delaporte, B., Schmitz, G., Le Moyne, L., "Development and validation of a 5 stroke engine for range extenders application", *Energy Conversion and Management* 82:259–267, 2014, doi: 10.1016/j.enconman.2014.03.025.
13. Arcidiacono, M., Baratta, M., Finesso, R., Kheshtinejad, H. et al., "Use of an Innovative Predictive Heat Release Model Combined to a 1D Fluid-Dynamic Model for the Simulation of a Heavy Duty Diesel Engine," *SAE Int. J. Engines* 6(3):1566-1579, 2013, doi:10.4271/2013-24-0012.
14. Baratta, M., Finesso, R., Misul, D., and Spessa, E., "Comparison between Internal and External EGR Performance on a Heavy Duty Diesel Engine by Means of a Refined 1D Fluid-Dynamic Engine Model," SAE Int. J. Engines 8(5):1977-1992, 2015, doi:10.4271/2015-24-2389
15. Baratta, M., Kheshtinejad, H.,, Laurenzano, D., Misul, D., et al., "Modelling aspects of a CNG injection system to predict its behavior under steady state conditions and throughout driving cycle simulations", *Journal of Natural Gas Science and Engineering* 24:52-63, doi: 10.1016/j.jngse.2015.03.010.
16. Montenegro, G., Onorati, A., Piscaglia, F., D'Errico, G., "Integrated 1D-MultiD Fluid Dynamic Models for the Simulation of I.C.E. Intake and Exhaust Systems", SAE Technical Paper 2007-01-0495, 2007, doi: 10.4271/2007-01-0495.
17. Rakopoulos, C. and Giakoumis, E., "Review of Thermodynamic Diesel Engine Simulations under Transient Operating Conditions," SAE Technical Paper 2006-01-0884, 2006, doi:10.4271/2006-01-0884.
18. Finesso, R., Spessa, E., and Yang, Y., "Development and Validation of a Real-Time Model for the Simulation of the Heat Release Rate, In-Cylinder Pressure and Pollutant Emissions in Diesel Engines," SAE Int. J. Engines 9(1):322-341, 2016, doi:10.4271/2015-01-9044.
19. Gani, E. and Manzie, C., "Indicated Torque Reconstruction from Instantaneous Engine Speed in a Six-cylinder SI Engine Using Support Vector Machines," SAE Technical Paper 2005-01-0030, 2005, doi:10.4271/2005-01-0030.
20. Asik, J., Peters, J., Meyer, G., and Tang, D., "Transient A/F Estimation and Control Using a Neural Network," SAE Technical Paper 970619, 1997, doi:10.4271/970619.
21. C. Bennett, J.F. Dunne, S. Trimby, D. Richardson, "Engine cylinder pressure reconstruction using crank kinematics and recurrently-trained neural networks", Mechanical systems and signal processing 85:126-145, 2016, doi: 10.1016/j.ymssp.2016.07.015.
22. Yusuf Cay, "Prediction of a gasoline engine performance with artificial neural network", Fuel 111:324-331, 2013, doi: 10.1016/j.fuel.2012.12.040.

23. Brusca, S., Lanzafame, R., and Messina, M., "A Combustion Model for ICE by Means of Neural Network," SAE Technical Paper 2005-01-2110, 2005, doi:10.4271/2005-01-2110.
24. Brahma, I., He, Y., and Rutland, C., "Improvement of Neural Network Accuracy for Engine Simulations," SAE Technical Paper 2003-01-3227, 2003, doi:10.4271/2003-01-3227.
25. Finesso, R., Spessa, E., Yang, Y., Alfieri, V. et al., "HRR and MFB50 Estimation in a Euro 6 Diesel Engine by Means of Control-Oriented Predictive Models," SAE Int. J. Engines 8(3):1055-1068, 2015, doi:10.4271/2015-01-0879.
26. Chmela, F.G., and Orthaber, G.C., "Rate of Heat Release Prediction for Direct Injection Diesel Engines Based on Purely Mixing Controlled Combustion", SAE Technical Paper 1999-01-0186, 1999, doi:10.4271/1999-01-0186.
27. Egnell, R., "A Simple Approach to Studying the Relation between Fuel Rate, Heat Release Rate and NO Formation in Diesel Engines", SAE Technical Paper 1999-01-3548, 1999, doi:10.4271/1999-01-3548.
28. Ryan, T. W., Callahan, T.J., "Homogeneous Charge Compression Ignition of Diesel Fuels". SAE Technical Paper 961160, 1996, doi:10.4271/961160.
29. Ericson, C., Westerberg, B., Andersson, M., and Egnell, R., "Modelling Diesel Engine Combustion and NOx Formation for Model Based Control and Simulation of Engine and Exhaust Aftertreatment Systems", SAE Technical Paper 2006-01-0687, 2006, doi:10.4271/2006-01-0687.
30. Catania, A.E., Finesso, R., Spessa, E., "Predictive Zero-Dimensional Combustion Model for DI Diesel Engine Feed-Forward Control", *Energy Conversion and Management.* 52(10):3159–3175, 2011, doi:10.1016/j.enconman.2011.05.003.
31. Heywood, J.B., "Internal Combustion Engine Fundamentals", McGraw-Hill Intern. Editions, 1988.
32. D'Ambrosio, S., Finesso, R., Fu, L., Mittica, A., Spessa, E., "A Control-Oriented Real-Time Semi-Empirical Model for the Prediction of NOx Emissions in Diesel Engines", *Applied Energy* 130:265-279; 2014,.doi: 10.1016/j.apenergy.2014.05.046
33. Chen, S.K., Flynn, P.F., "Development of Single Cylinder Compression Ignition Research Engine", SAE Technical Paper 650733, 1966. doi:10.4271/650733.
34. Finesso, R. and Spessa, E., "Real-Time Predictive Modeling of Combustion and NOx Formation in Diesel Engines Under Transient Conditions," SAE Technical Paper 2012-01-0899, 2012, doi:10.4271/2012-01-0899.

Contact Information

Prof. Ezio Spessa

IC Engines Advanced Laboratory

Dipartimento Energia, Politecnico di Torino

c.so Duca degli Abruzzi, 24 - 10129 Torino (Italy)

phone: +39-011-090.4482

ezio.spessa@polito.it.

Definitions/Abbreviations

ANN	Artificial neural network
BMEP	Brake Mean Effective Pressure
CA	crank angle
CFD	Computer Fluid-Dynamics
c_p	specific heat at constant pressure
c_v	specific heat at constant volume
DT	Dwell-time
ECU	Engine Control Unit
EGR	Exhaust Gas Recirculation
EOC	end of Combustion
EOI	end of injection
EVO	Exhaust Valve Opening
FMEP	Friction Mean Effective Pressure
FPT	Fiat Powertrain Technologies
h	Specific enthalpy
H_{abs}	absolute humidity of the air
H_L	lower heating value of the fuel
HiL	Hardware-in-the-Loop
HRR	Heat Release Rate
ICEAL-PT	Internal Combustion Engines Advanced Laboratory at the Politecnico di Torino
IMEP	Indicated Mean Effective Pressure
IMEP360	Gross Indicated Mean Effective Pressure
IMEP720	Net Indicated Mean Effective Pressure

IVC	Intake Valve Closing
K	combustion rate coefficient
m	mass; compression phase polytropic coefficient
$\mathbf{m_{f,inj}}$	total injected fuel mass per cycle/cylinder
m'	expansion phase polytropic coefficient
$\dot{m}_{f,inj}$	fuel injection rate
MFB50	crank angle at which 50% of the fuel mass fraction has burned
n	engine rotational speed
$\mathbf{O_2}$	intake charge oxygen concentration
p	pressure
$\mathbf{p_{exh}}$	exhaust manifold pressure
$\mathbf{p_f}$	injection pressure
PFP	Peak firing pressure
$\mathbf{p_{int}}$	intake manifold pressure
$\mathbf{p_{IVC}}$	In-cylinder pressure at IVC
pil	pilot injection
PMEP	Pumping Mean Effective Pressure
q	injected fuel volume quantity
$\mathbf{Q_{ch}}$	chemical heat release
$\mathbf{Q_{f,evap}}$	energy associated to fuel evaporation
$\mathbf{Q_{fuel}}$	chemical energy associated with the injected fuel
$\mathbf{Q_{ht}}$	heat transfer between the charge and the walls
$\mathbf{Q_{ht,glob}}$	global heat transfer between the charge and the walls over the combustion interval
$\mathbf{Q_{net}}$	net heat release
$\mathbf{q_{f,inj}}$	total injected fuel volume quantity per cycle/cylinder
$\mathbf{q_{pil}}$	injected fuel volume quantity of the pilot injection
$\mathbf{q_{pil,tot}}$	total injected fuel volume quantity of the pilot injections
$\mathbf{R^2}$	squared correlation coefficient
RMSE	root mean square error
SOC	start of combustion
SOI	electric Start Of Injection
$\mathbf{SOI_{main}}$	electric Start Of Injection of the main pulse
SVM	Support vector machine
t	time
T	temperature
$\mathbf{T_{b,MFB50}}$	temperature of the burned gas zone at MFB50
tgt	target
$\mathbf{T_{int}}$	intake manifold temperature
V	volume
VGT	Variable Geometry Turbocharger

Greek symbols

$\boldsymbol{\varepsilon_{BMEP}}$	BMEP error threshold to stop iterations for model inversion
$\boldsymbol{\varepsilon_{NOx}}$	NOx error threshold to stop iterations for model inversion
$\gamma = c_p/c_v$	specific heat ratio
$\boldsymbol{\rho}$	density
$\boldsymbol{\rho_{SOI}}$	in-chamber ambient density evaluated at the SOI instant
$\boldsymbol{\rho_{SOC}}$	in-chamber ambient density evaluated at the SOC instant

τ	ignition delay coefficient
τ_{main}	ignition delay coefficient of the main pulse
τ_{pil}	ignition delay coefficient of the pilot pulse